

# Multifractal and complex network analyses of protein molecular dynamics

Yuan-Wu Zhou<sup>1,2</sup>, Jin-Long Liu<sup>1</sup>, Zu-Guo Yu<sup>1,3\*</sup>, Zhi-Qin Zhao<sup>1</sup> and Vo Anh<sup>3</sup>

<sup>1</sup>Hunan Key Laboratory for Computation and Simulation in Science and Engineering and Key Laboratory of Intelligent Computing and Information Processing of Ministry of Education, Xiangtan University, Xiangtan, Hunan 411105, China.

<sup>2</sup>Civil Construction Engineering Department, Guangxi University of Science and Technology, Liuzhou 545006, China.

<sup>3</sup>School of Mathematical Sciences, Queensland University of Technology, GPO Box 2434, Brisbane, Q4001, Australia.

## Abstract

Based on protein molecular dynamics, we analyze fractal properties of energy, pressure and volume time series using the multifractal detrended fluctuations analysis (MF-DFA); and investigate the topological and multifractal properties of their visibility graph (complex network) representations. The energy terms of proteins we considered are bonded potential, angle potential, dihedral potential, improper potential, kinetic energy, Van der Waals potential, electrostatic potential, total energy and potential energy. Results of MF-DFA show that these time series are multifractal. The numerical values of the exponent  $h(2)$  of MF-DFA which is related to Hurst exponent  $H$  show that the series of total energy and potential energy are non-stationary and anti-persistent; other kinds of time series are stationary and persistent apart from series of pressure which has the weakest memorability with  $H \approx 0.5$ . Results of complex networks analysis based on visibility graph algorithm show that these visibility graphs are exponential. Our numerical results of multifractal analysis of the visibility graphs show that multifractality exists in these networks. We also found that after taking average over all proteins, there is a linear relationship between  $\langle h(2) \rangle$  (from MF-DFA on time series) and  $\langle D(0) \rangle$  of the constructed visibility graphs for different energy, pressure and volume.

**Key words:** protein molecular dynamics; multifractal analysis; complex network; memorability; visibility graph.

**PACS:** 05.45.Df, 64.60.al, 87.15.H-

## 1 Introduction

Proteins are one of the most important biomacromolecules because they can carry out biological functions. The biological functions of proteins are usually determined by their structures. But

---

\*The contributions of the first two authors are equal, so Jin-Long Liu can be regarded as joint first author.  
Corresponding to: yuzg1970@yahoo.com

only structures of 97362 proteins (updated in Protein Data Bank [1] on 2014-01-28) have been obtained by experimental methods, such as X-ray (88.4%), solution NMR (10.6%) and electron microscopy (0.7%). Even so, these experimental methods can only give static structures which are dead structures. On the other hand, protein molecular dynamics is an effective way to give live structures. Some researchers used theoretical molecules, for example, polyalanines for modelling  $\alpha$ -helices [2–6]. NAMD (*Not (just) Another Molecular Dynamics program*) [7] is a freeware molecular dynamics simulation package. Based on the NAMD software, Rueda *et al.* analyzed the molecular dynamics of 30 real proteins [8]. Using protein molecular dynamics, we can get some time series. The features of these series are determined by protein structures. Protein molecule energy includes kinetic energy and potential energy, and potential energy can be calculated by quasi-empirical way, such as CHARMM [9] and AMBER [10].

Fractal methods can be used to characterize the scaling properties of time series. Fractal methods have been used to investigate proteins (see [11] for review). But the fractal analysis is not enough when the object studied can not be described by a single fractal dimension. Multifractals are a broad generalization of the (geometrical) fractals. Multifractal analysis was initially proposed to treat turbulence data and is a useful way to characterize the spatial heterogeneity of both theoretical and experimental fractal patterns [12]. The multifractal detrended fluctuations analysis (MF-DFA) is a good tool to characterize the multifractal property and long-range correlation in time series [13]. Multifractal analysis has been used to study genomes [14–16], protein structures and functions (e.g. [17–21]). In this paper, we will analyze time series of energy, pressure and volume using MF-DFA [13] for real proteins.

In last decade, the study of networks has become a blossoming area in science across many disciplines. Network theory has become a powerful tool to analyze protein complex structure. Single protein in 3D space can also be considered as biological complex systems emerged through the interactions of their constituent amino acids. These interactions among the amino acids within a protein can be presented as residues interaction network (RIN) (or called residues interaction graphs (RIGs), protein contact network (PCN), protein structure network (PSN), protein contact map (PCM), amino acid network (AAN), which can be constructed with varying definitions of nodes and edges [22–24]. Recent studies have shown that complex network theory (such as recurrence networks) may be an effective method to extract the information embedded in time series [25–29]. The visibility graph algorithm can convert time series into complex networks [30,31]. The graph inherits several properties of the time series in its structure. We can understand time series from a new point of view using visibility graph. In this paper, we will analyze time series of energy, pressure and volume using visibility graph algorithm [30] for real proteins.

Song *et al.* [32,33] proposed an algorithm to calculate the fractal dimension of complex networks which can unfold their self-similar property. They mentioned that the box counting fractal analysis is an effective tool for the further study of complex networks. Kim *et al.* [34] proposed a random sequential box-counting algorithm to estimate the fractal dimension of networks. Lee and Jung [35] found that MFA is the best tool to describe the probability distribution of the clustering coefficient of a complex network. Furuya and Yakubo [36] analytically and numerically demonstrated the

possibility that the fractal property of a scale-free network cannot be characterized by a single fractal dimension when the network takes a multifractal structure. Almost at the same time, Wang *et al.* [37] adopted the modified fixed-size box-counting algorithm to detect the multifractal behavior of some theoretical and real networks, such as scale-free networks, small-world networks, random networks, and protein-protein interaction (PPI) networks of different species. Their numerical results indicated that multifractality exists in scale-free networks and PPI networks, while for small-world networks and random networks their multifractality is not clear-cut. Recently Li *et al.* [38] improved the modified fixed-size box-counting algorithm for multifractal analysis of networks and studied the multifractal properties of a family of fractal networks introduced by Gallos *et al.* [39]. The new algorithm proposed by our group (Li *et al.* [38]) has been used to investigate the topological and fractal properties of the recurrence networks constructed from fractional Brownian motions (Liu *et al.* [40]). In this paper, we will also analyze multifractal properties of the constructed visibility graphs of the time series of energy, pressure and volume using the new algorithm proposed by our group (Li *et al.* [38]).

## 2 Molecular dynamics for protein

The behavior of biomolecular systems can be modelled by molecular dynamics, and molecular dynamics is helpful to understand protein functions. Usually, procedure of molecular dynamics for proteins is as follow:

(a). Initialize the positions and velocities of all atoms. The initial positions of atoms come from Protein Data Bank (PDB [1]). Add water and ions to a box with protein, minimize the box system energy. Then, the initial velocities of atoms are assigned from the Maxwell's distribution.

(b). Calculate forces for all atoms using potential energy. Usually, the protein potential energy can be defined as:

$$V = V_{bonds} + V_{angles} + V_{dihedrals} + V_{impropers} + V_{Vdw} + V_{electrostatic}, \quad (1)$$

where  $V$  is protein potential energy,  $V_{bonds}$  is bonded potential,  $V_{angles}$  is angle potential,  $V_{dihedrals}$  is dihedral potential,  $V_{impropers}$  is improper potential,  $V_{Vdw}$  is Van der Waals potential, and  $V_{electrostatic}$  is electrostatic potential. In this paper, we analyze potential energy and kinetic energy time series. Then, forces that act on an atom can be written as follow:

$$\vec{F} = \frac{\partial V(\vec{r})}{\partial \vec{r}}, \quad (2)$$

where  $\vec{r}$  is the position vector of atoms.

(c). Apply thermostat and volume changes.

(d). Update positions and velocities, go to step (b) till termination condition meet. According to Newton's law, kinetic equation can be written as:

$$\vec{F} = m \frac{\partial^2 \vec{r}}{\partial t^2}. \quad (3)$$

Using an algorithm, such as Verlet algorithm or LeapFrog algorithm, new positions and velocities can be calculated.

(e). Analyze data. NAMD is a software for biomolecular molecular dynamics [7]. Some researchers used NAMD to achieve important results [8]. In the paper, we use it to simulate protein dynamics.

### 3 Multifractal detrended fluctuation analysis for time series

In order to characterize multifractal property of stationary or nonstationary time series, MF-DFA [13] is an effective method. This approach can be described as follow. Given a time series  $x_k$ ,  $k = 1, \dots, N$ , where  $N$  is the length of the series. The profile  $Y(i)$  is defined as

$$Y(i) \equiv \sum_{k=1}^i [x_k - \langle x \rangle]. \quad i = 1, \dots, N, \quad (4)$$

$\langle x \rangle$  is the mean of sequence  $x_k$ . Then  $Y(i)$  is divided into  $N_s \equiv \text{int}(N/s)$  non-overlapping and continuous segments of equal length  $s$ . Then we calculate the variance by

$$F^2(s, v) \equiv \frac{1}{s} \sum_{i=1}^s \{Y[(v-1)s+i] - y_v(i)\}^2, \quad (5)$$

for each segment  $v$ ,  $v = 1, \dots, N$  and

$$F^2(s, v) \equiv \frac{1}{s} \sum_{i=1}^s \{Y[N - (v - N_s)s + i] - y_v(i)\}^2, \quad (6)$$

for  $v = N_s + 1, \dots, 2N_s$ , where  $y_v(i)$  is the fitting polynomial in segment  $v$  (linear, quadratic, cubic, or higher order polynomials). Last we take average over  $2N_s$  segments to achieve the  $q$ th order fluctuation function

$$F_q(s) \equiv \left\{ \frac{1}{2N_s} \sum_{v=1}^{2N_s} [F^2(s, v)]^{q/2} \right\}^{1/q}, \quad (\text{if } q \neq 0). \quad (7)$$

$$F_q(s) \equiv \exp\left\{ \frac{1}{4N_s} \sum_{v=1}^{2N_s} \ln[F^2(s, v)] \right\}, \quad (\text{if } q = 0). \quad (8)$$

We will assume that  $F_q(s)$  is characterized by a power law:

$$F_q(s) \propto s^{h(q)}. \quad (9)$$

The scaling function  $h(q)$  is then determined by the regression of  $\log F_q(s)$  on  $\log s$  in some range of time scale  $s$ .

For fractional Brownian motion, Movahed *et al.* [41] showed that the Hurst index  $H = h(2) - 1$ . Using this relationship (or  $H = h(2)$  for the stationarity case) and the estimate of  $h(2)$  from the regression of  $\log F_2(s)$  on  $\log s$ , an estimate of the Hurst index  $H$ , and hence the extent of long memory in the time series, is obtained. For Brownian motion (with uncorrelated increments), the scaling exponent  $H$  is equal to  $1/2$ . The range  $1/2 < H < 1.0$  indicates the presence of long memory/persistence, while the range  $0 < H < 1/2$  indicates short memory/anti-persistence.

## 4 Complex networks: visibility graph for time series

A graph (or network) is a collection of nodes, which denote the elements of a system, and links or edges, which identify the relations or interactions among these elements.

Inspired by the concept of visibility [42], Lacasa *et al.* [30] suggested a simple computational method to convert a time series into a graph, known as visibility graph (VG). A visibility graph is obtained from the mapping of a time series into a network according to the following visibility criterion: Given a time series  $\{x_1, x_2, \dots, x_N\}$ , two arbitrary data points  $x_{t_a}$  and  $x_{t_b}$  in the time series have visibility, and consequently become two connected nodes in the associated graph, if any other data point  $x_{t_c}$  such that  $t_a < t_c < t_b$  fulfils

$$x_{t_c} < x_{t_a} + (x_{t_b} - x_{t_a}) \frac{t_c - t_a}{t_b - t_a}; \quad (10)$$

thus a connected, unweighted network could be constructed from a time series and is called its *visibility graph*. It has been shown [30] that time series structures is inherited in the associated graph, such that periodic, random, and fractal series map into motif-like random exponential and scale-free networks, respectively. If the degree distribution  $P(k)$  for a network follows  $P(k) \propto k^{-\alpha}$ , the network is scale-free. If the degree distribution  $P(k)$  for a network follows  $P(k) \propto \exp(-\lambda k)$ , the network is exponential. The greater value of  $\lambda$ , the faster attenuation of  $P(k)$  is along with  $k$ . We can find characteristics of time series from a different perspective using visibility graph.

## 5 Multifractal analysis of complex networks

In recent years, the multifractal analysis was applied to study the complex networks and has made some progress.

Fixed-size box-covering algorithm proposed by Halsey *et al.* [12] is one of the most common methods of multifractal analysis. For a given measure  $\mu$  with support set  $E$  in a metric space, we consider the partition sum

$$Z_r(q) = \sum_{\mu(B) \neq 0} [\mu(B)]^q, \quad (11)$$

where  $q \in \mathbb{R}$  and the sum runs over all different nonempty boxes  $B$  of a given size  $r$  in a covering of the support set  $E$ . From the definition above, we can obtain  $Z_r(q) \geq 0$  and  $Z_r(0) = 1$ . The exponent  $\tau(q)$  of the measure  $\mu$  can be defined as

$$\tau(q) = \lim_{r \rightarrow 0} \frac{\ln Z_r(q)}{\ln r}, \quad (12)$$

and the generalized fractal dimensions of the measure  $\mu$  are defined as

$$D(q) = \frac{\tau(q)}{q - 1}, \quad (13)$$

for  $q \neq 1$ , and

$$D(q) = \lim_{r \rightarrow 0} \frac{Z_{1,r}}{\ln r}, \quad (14)$$

for  $q = 1$ , where  $Z_{1,r} = \sum_{\mu(B) \neq 0} \mu(B) \ln \mu(B)$ . The linear regression of  $[\ln Z_r(q)]/(q - 1)$  against  $\ln r$  for  $q \neq 1$  gives numerical estimates of the generalized fractal dimensions  $D(q)$ , and similarly a

linear regression of  $Z_{1,r}$  against  $\ln r$  for  $q = 1$ . In particular,  $D(0)$  is the box-counting dimension (or fractal dimension),  $D(1)$  is the information dimension and  $D(2)$  is the correlation dimension. If the  $\tau(q)$  or  $D(q)$  curve versus  $q$  is a straight line, the object is monofractal. However, if this curve is convex, the object is multifractal.

In order to calculate the exponent  $\tau(q)$  and the generalized fractal dimensions  $D(q)$  and then study the multifractality of networks, the measure  $\mu$  of each box is usually defined as the ratio of the number of nodes covered by the box and the total number of nodes in the entire network. Wang *et al.* [37] proposed a modified fixed-size box-counting algorithm to calculate the  $\tau(q)$  and  $D(q)$  and then investigated the multifractal behavior of complex networks. Then Li *et al.* [38] improved the modified fixed-size box-counting algorithm for multifractal analysis of networks. The improved algorithm can be summarized as follows:

- (i) Initially, make sure all nodes in the entire network are not covered and no node is selected as a center of a box.
- (ii) According to the size  $N$  of networks constructed, set  $t = 1, 2, \dots, 1000$  appropriately. Rearrange the nodes into 1000 different random orders. More specifically, in each random order, nodes which will be selected as a center of a box are randomly arrayed.
- (iii) Set the radius  $r$  of the box which will be used to cover the nodes in the range  $r \in [1, d]$ , where  $d$  is the diameter of the network.
- (iv) Treat the nodes in the  $t$ -th random order that we got in (ii) as the center of a box, search all the neighbor nodes by distance  $r$  from the center and cover all nodes which are found but have not been covered yet.
- (v) If no newly covered nodes have been found, then this box is discard.
- (vi) Repeat Steps (iv) and (v) until all the nodes are covered by the corresponding boxes. We denote the number of boxes in this box covering as  $N(t, r)$ .
- (vii) Repeat Steps (iv) to (vi) for all 1000 random orders to find a box covering with minimal number of boxes  $N(t, r)$ .
- (viii) For the nonempty boxes  $B$  in the first box covering with minimal number of boxes  $N(t, r)$ , define the measure of this box as  $\mu(B) = N_B/N$ , where  $N_B$  is the number of nodes covered by the box  $B$ , and  $N$  is the size of the network. Then we calculate the partition sum  $Z_r(q) = \sum_{\mu(B) \neq 0} [\mu(B)]^q$ .
- (ix) For different value of  $r$ , repeat Steps (iii) to (viii) to calculate the partition sum  $Z_r(q)$  and then use the  $Z_r(q)$  for linear regression.

A key step of linear regression is to obtain the appropriate range of  $r \in [r_{\min}, r_{\max}]$ . Then we calculate the exponents  $\tau(q)$  and generalized fractal dimensions  $D(q)$  in the scaling ranges. In our calculation, we obtain the generalized fractal dimensions through a linear regression of

$[\ln Z_r(q)]/(q-1)$  against  $\ln(r/d)$  for  $q \neq 1$ , and similarly a linear regression of  $Z_{1,r}$  against  $\ln(r/d)$  for  $q = 1$ , where  $Z_{1,r} = \sum_{\mu(B) \neq 0} \mu(B) \ln \mu(B)$ .

## 6 Results and discussion

We use a list of 29 proteins (without ligands, RNA, or DNA, greater than 100 amino acids) as [8] to simulate the dynamics of them (see Table 1).

Using NAMD with energy step size  $200fs$ , equilibrated structures are used as starting points for 10-ns production trajectories, performed at constant pressure (1atm) and temperature (310K) using standard coupling schemes (the same in all cases). CHARMM force fields are used in production runs. Then, we get time series of bonded potential, angle potential, dihedral potential, improper potential, electrostatic potential, Van der Waals potential, kinetic energy, total energy, potential energy, pressure, and volume. For example, we give the 11 time series of protein 1A3H in Figures 1 to 3.

Then we perform MF-DFA on these time series. We give the  $h(q)$  curves of 11 time series for protein 1A3H in Figure 4 as an example. From the  $h(q)$  curves of these time series for all proteins, we found that all time series considered here are multifractal. In particular, the numerical values of  $h(2)$  which is related to Hurst exponent  $H$  are given in Table 2. The average values of  $h(2)$  and standard deviations for all 11 items of 29 proteins are given in Table 3.

For energy terms, energy values are in *kcal/mol*, bonded potential  $\sim 10^3$ , angle potential  $\sim 10^3$ , dihedral potential  $\sim 10^3$ , improper potential  $\sim 10^2$ , electrostatic potential  $\sim 10^5$ , Van der Waals potential  $\sim 10^4$ , kinetic energy  $\sim 10^4$ , total energy  $\sim 10^5$ , and potential energy  $\sim 10^5$ . From Table 3, we can see that the series of total energy and potential energy are non-stationary ( $h(2) > 1.0$ ) and anti-persistent ( $0 < H = h(2) - 1 < 0.5$ ). Other kinds of time series are stationary and persistent apart from series of pressure which has the weakest memorability with  $H \approx 0.5$ . Among bonded potential, angle potential, dihedral potential, and improper potential, we can see that the series of angle potential have the strongest memorability and those of improper potential have the weakest, and the memorability of those of dihedral potential is greater than those of bonded potential. Among the three largest energy terms, electrostatic potential, Vdw potential and kinetic energy, we find that the long-range correlation of the series of electrostatic potential is the strongest and that of series of Vdw potential is the weakest. The energy is related with protein conformation. Stronger memorability means to keep protein conformation easier.

Then, these time series are converted into visibility graphs. We denote  $k$  the degree of nodes,  $P(k)$  the probability of degree  $k$ . We obtain  $k \sim P(k)$ ,  $\log(k) \sim \log(P(k))$ , and  $k \sim \log(P(k))$  relation plots and found that only the linearity of  $k \sim \log(P(k))$  relation plots are good (The plot of protein 1A3H is given in Figure 5 as an example). So the visibility graphs of these terms are exponential networks. We give the numerical values of exponent  $\lambda$  in Table 4. Among of the three largest energy terms, electrostatic potential, Vdw potential and kinetic energy, the attenuation of electrostatic potential degree distribution is the fastest. Total energy has the fastest attenuation among all energy terms. Potential energy has the faster attenuation comparing to its components.

In our paper, we try to reveal the relationship between time series and its related visibility graph from the perspective of network structure and then further to understand the biological functions of these proteins. We probe the multifractal behavior of visibility graphs using the improved algorithm described in Section 5. As an example, we show the  $\tau(q)$  curves and  $D(q)$  curves of protein 1A3H in Figures 6 and 7, respectively. From Figures 6 and 7, we find that the  $\tau(q)$  and  $D(q)$  curves of visibility networks are not straight lines. So the multifractality exists in these visibility graphs constructed from time series of energy, pressure and volume for protein 1A3H. We also found that the visibility networks of other time series for all 29 proteins exhibit multifractality. From this point of view, the multifractality of energy, pressure and volume time series of proteins is inherited in their visibility graphs. For 29 time series (29 proteins) of each kind of energy (or pressure or volume), we calculated the average value of  $h(2)$  (from MF-DFA on time series) and  $D(0)$  the constructed visibility graphs over the 29 proteins. Hence we got 11 values of  $\langle h(2) \rangle$  and 11 values of  $\langle D(0) \rangle$  respectively. Finally we found that there is a linear relationship between  $\langle h(2) \rangle$  and  $\langle D(0) \rangle$  as shown in Figure 8. The relationship can be fitted by following linear formula:

$$\langle D(0) \rangle = 1.041 * \langle h(2) \rangle + 4.3637.$$

## 7 Conclusions

Using NAMD software, we got time series of bonded potential, angle potential, dihedral potential, improper potential, electrostatic potential, Van der Waals potential, kinetic energy, total energy, potential energy, pressure, and volume for each protein. The results of MF-DFA on these time series show that all of them are multifractal.

In particular, the numerical values of  $h(2)$  of MF-DFA which is related to Hurst exponent  $H$  show that the series of total energy and potential energy are non-stationary and anti-persistent; other kinds of time series are stationary and persistent apart from series of pressure which has the weakest memorability with  $H \approx 0.5$ .

It is also found that the constructed visibility graphs of these series are exponential networks. The multifractality exists in these constructed visibility graphs. From this point of view, the multifractality of energy, pressure and volume time series of proteins is inherited in their visibility graphs.

After taking average over all proteins, we found that there is a linear relationship between  $\langle h(2) \rangle$  (from MF-DFA on time series) and  $\langle D(0) \rangle$  of constructed visibility graphs for different energy, pressure and volume.

## Acknowledgments

This project was supported by the Natural Science Foundation of China (Grant No. 11371016), the Chinese Program for Changjiang Scholars and Innovative Research Team in University (PCSIRT) (Grant No. IRT1179); the Research Foundation of Education Commission of Hunan Province of



China (Grant No. 11A122); the Lotus Scholars Program of Hunan province of China; postdoctoral research fund of Xiangtan University of China.

## References

- [1] H.M. Berman, J. Westbrook, Z. Feng, G. Gilliland, T.N. Bhat, H. Weissig, I.N. Shindyalov, and P.E. Bourne, The protein data bank, *Nucleic acids research*, 28(1) (2000) 235-242.
- [2] M.A. Moret, P.M. Bisch, K.C. Mundim, and P.G. Pascutti, New Stochastic Strategy to Analyze Helix Folding, *Biophys. J.*, 82(3) (2002) 1123-1132.
- [3] F.P. Agostini, O. Soares-Pinto Dde, M.A. Moret, C. Osthoff, and P.G. Pascutti, Generalized simulated annealing applied to protein folding studies, *J. Comput. Chem.*, 27(11) (2006) 1142-1155.
- [4] P.H. Figueiredo, E. Nogueira Jr., M.A. Moret, and S. Coutinho, Multifractal analysis of polyalanines time series, *Physica A*, 389(10) (2010) 2090-2095.
- [5] P.H. Figueiredo, M.A. Moret, P.G. Pascutti, E. Nogueira Jr., and S. Coutinho, Self-affine analysis of protein energy, *Physica A*, 389(13) (2010) 2682-2686.
- [6] M.A. Moret, P.G. Pascutti, K.C. Mundim, P.M. Bisch, and E. Nogueira Jr., Multifractality, Levinthal paradox, and energy hypersurface, *Phys. Rev. E*, 63 (2001) 020901.
- [7] J.C. Phillips, R. Braun, W. Wang, J. Gumbart, E. Tajkhorshid, E. Villa, C. Chipot, R.D. Skeel, L. Kale, and K. Schulten, Scalable molecular dynamics with NAMD, *J. Comput. Chem.*, 26(16) (2005) 1781-1802.
- [8] M. Rueda, C. Ferrer-Costa, T. Meyer, A. Perez, J. Camps, A. Hospital, J.L. Gelpi, and M. Orozco, A consensus view of protein dynamics, *Proc. Natl. Acad. Sci. U.S.A.*, 104(3) (2007) 796-801.
- [9] B.R. Brooks, C.L. Brooks, A.D. MacKerell Jr., *et al.*, CHARMM: the biomolecular simulation program, *J. Comput. Chem.*, 30(10) (2009) 1545-1614.
- [10] D.A. Case, T.E. Cheatham, T. Darden, H. Gohlke, R. Luo, K.M. Merz Jr., A. Onufriev, C. Simmerling, B. Wang, and R.J. Woods, The Amber biomolecular simulation programs, *J. Comput. Chem.*, 26(16) (2005) 1668-88.
- [11] A. Banerji and I. Ghosh, Fractal symmetry of protein interior: What have we learned?, *Cell. Mol. Life Sci.*, 68 (2011) 2711-2737.
- [12] T.C. Halsey, M.H. Jensen, L.P. Kadanoff, I. Procaccia, and B.I. Shraiman, Fractal measures and their singularities: the characterization of strange sets, *Phys. Rev. A*, 33 (1986) 1141-1151.
- [13] J.W. Kantelhardt, S.A. Zschiegner, E. Koscielny-Bunde, A. Bunde, S. Havlin, and H.E. Stanley, Multifractal detrended fluctuation analysis of nonstationary time series, *Physica A*, 316(1) (2002) 87-114.
- [14] Z.G. Yu, V. Anh, and K.S. Lau, Measure representation and multifractal analysis of complete genome, *Phys. Rev. E*, 64 (2001) 031903 .
- [15] Z.G. Yu, V. Anh, and K.S. Lau, Multifractal and correlation analysis of protein sequences from complete genome, *Phys. Rev. E*, 68 (2003) 021913.
- [16] Z.G. Yu, V. Anh, and K.S. Lau, Chaos game representation, and multifractal and correlation analysis of protein sequences from complete genome based on detailed HP model, *J. Theor. Biol.*, 226 (2004) 341-348.
- [17] J.S. Balafas and T.G. Dewey, Multifractal analysis of solvent accessibilities in proteins, *Phys. Rev. E.*, 52 (1995) 880-887.

- [18] Z.G. Yu, V. Anh, K.S. Lau, and L.Q. Zhou, Fractal and multifractal analysis of hydrophobic free energies and solvent accessibilities in proteins, *Phys. Rev. E.*, 73 (2006) 031920.
- [19] J.Y. Yang, Z.G. Yu, and V. Anh, Clustering structure of large proteins using multifractal analyses based on 6-letters model and hydrophobicity scale of amino acids, *Chaos, Solitons and Fractals*, 40 (2009) 607-620.
- [20] J.Y. Yang, Z.L. Peng, Z.G. Yu, R.J. Zhang, V. Anh, and D. Wang, Prediction of protein structural classes by recurrence quantification analysis based on chaos game representation, *J. Theor. Biol.*, 257 (2009) 618-626.
- [21] S.M. Zhu, Z.G. Yu, and V. Anh, Protein structural classification and family identification by multifractal analysis and wavelet spectrum, *Chin. Phys. B*, 20 (2011) 010505.
- [22] G. Amitai, A. Shemesh, E. Sitbon, M. Shklar, D. Netanel, I. Venger, and S. Pietrokovski, Network analysis of protein structure identifies functional residue, *J. Mol. Biol.*, 344 (2004) 1135-1146.
- [23] A.R. Atilgan, P. Akan, and C. Baysal, Small-World communication of residues and significance for protein dynamics, *Biophys. J.*, 86 (2004) 85-91.
- [24] G. Bagler and S. Sinha, Network properties of protein structures, *Physica A*, 346 (2005) 27-33.
- [25] R.V. Donner, Y. Zou, J.F. Donges, N. Marwan, and J. Kurths, Recurrence networks: a novel paradigm for nonlinear time series analysis, *New J. Phys.*, 12 (2010) 033025.
- [26] R.V. Donner, Y. Zou, J.F. Donges, N. Marwan, and J. Kurths, Ambiguities in recurrence-based complex network representations of time series, *Phys. Rev. E*, 81 (2010) 015101(R).
- [27] R.V. Donner, J. Heitzig, J.F. Donges, Y. Zou, N. Marwan, and J. Kurths, The geometry of chaotic dynamics C a complex network perspective, *Eur. Phys. J. B*, 84 (2011) 653-672.
- [28] R.V. Donner, M. Small, J.F. Donges, N. Marwan, Y. Zou, R. Xiang and J. Kurths, Recurrence-based time series analysis by means of complex network methods, *Int. J. Bifurc. and Chaos*, 21(4) (2011) 1019-1046.
- [29] J.F. Donges, J. Heitzig, R.V. Donner, and J. Kurths, Analytical framework for recurrence network analysis of time series, *Phys. Rev. E*, 85 (2012) 046105.
- [30] L. Lacasa, B. Luque, F. Ballesteros, J. Luque, and J.C. Nuño, From time series to complex networks: The visibility graph, *Proc. Natl. Acad. Sci. U.S.A.*, 105(13) (2008) 4972-4975.
- [31] L. Lacasa and R. Toral, Description of stochastic and chaotic series using visibility graphs, *Phys. Rev. E*, 82 (2010) 036120.
- [32] C. Song, S. Havlin and H.A. Makse, Self-similarity of complex networks, *Nature*, 433 (2005) 392-395.
- [33] C. Song, L.K. Gallos, S. Havlin and H.A. Makse, How to calculate the fractal dimension of a complex network: the box covering algorithm, *J. Stat. Mech.: Theor. Exp.*, 3 (2007) P03006.
- [34] J.S. Kim, K.I. Goh, G. Salvi, E. Oh, B. Kahng and D. Kim, Fractality in complex networks: Critical and supercritical skeletons, *Phys. Rev. E*, 75 (2007) 016110.
- [35] C.Y. Lee and S.H. Jung, Statistical self-similar properties of complex networks, *Phys. Rev. E*, 73 (2006) 066102.
- [36] S. Furuya and K. Yakubo, Multifractality of complex networks, *Phys. Rev. E*, 84 (2011) 036118.
- [37] D.L. Wang, Z.G. Yu and V. Anh, Multifractal analysis of complex networks, *Chin. Phys. B*, 21 (2012) 080504.
- [38] B.G. Li, Z.G. Yu and Y. Zhou, Fractal and multifractal properties of a family of fractal networks, *J. Stat. Mech.: Theor. Exp.*, 2014 (2014) P02020.

- [39] L.K. Gallos, C. Song, S. Havlin and H.A. Makse, Scaling theory of transport in complex biological networks, *Proc. Natl. Acad. Sci. U.S.A.*, 104 (2007) 7746-7751.
- [40] J.L. Liu, Z.G. Yu and V. Anh, Topological properties and fractal analysis of recurrence network constructed from fractional Brownian motions, *Phys. Rev. E*, (Accepted for publication) (2014).
- [41] M.S. Movahed, G.R. Jafari, F. Ghasemi, S. Rahvar, and M.R.R. Tabar, Multifractal detrended fluctuation analysis of sunspot time series, *J. Stat. Mech.: Theory exper.* 2 (2006) P02003.
- [42] M. de Berg, M. van Kreveld, M. Overmans, and O. Schwarzkopf: *Computational Geometry: Algorithms and Applications*(Third Edition), Springer-Verlag, Berlin, 2008.

Table 1: Structures representative of protein dynamics

PDB ID code	The number of amino acids	Helical (%)	Beta sheet (%)	Exp structure
1A3H	300	38	19	X-ray
1BFG	126	8	35	X-ray
1BSN	138	26	37	NMR
2DN8	100	0	37	NMR
2DO7	101	43	9	NMR
1F39	101	3	39	X-ray
1FE6	108	90	0	X-ray
1FPR	294	30	19	X-ray
1H6T	291	17	28	X-ray
1I4S	294	68	1	X-ray
1IQQ	200	29	20	X-ray
1JLI	112	58	0	NMR
1K40	126	86	0	X-ray
1KS9	291	47	19	X-ray
1KTE	105	50	19	X-ray
1KUU	202	20	38	X-ray
1KXA	159	5	47	X-ray
1MIX	206	39	18	X-ray
1MJY	350	20	33	X-ray
1N12	298	4	55	X-ray
1OO9	294	25	17	NMR
1OOI	124	66	1	X-ray
1PHN	334	76	0	X-ray
1RAL	308	36	15	X-ray
1SUR	215	48	14	X-ray
1WUZ	103	12	34	NMR
1WWB	103	2	49	X-ray
1X0M	403	47	15	X-ray
1XGO	295	30	22	X-ray

Table 2: Exponent  $h(2)$  of time series for 29 proteins

PDB ID	Bond-p	ang-p	dih-p	imp-p	ele-p	Vdw-p	Kin-e	Tot-e	Pot-e	pre	vol
1A3H	0.6241	0.7405	0.6954	0.59	0.9046	0.6279	0.841	1.2465	1.0306	0.4758	0.8672
1BFG	0.6244	0.7484	0.7263	0.577	0.8857	0.6023	0.8367	1.2336	1.0261	0.4833	0.8443
1BSN	0.6223	0.7594	0.7365	0.5611	0.8937	0.5997	0.837	1.2522	1.0391	0.4964	0.8651
2DN8	0.6386	0.7578	0.7535	0.5805	0.9114	0.6414	0.8372	1.2581	1.0408	0.5214	0.8281
2DO7	0.622	0.7604	0.7481	0.5681	0.9108	0.6303	0.8364	1.2599	1.0404	0.5221	0.8415
1F39	0.6377	0.7401	0.7329	0.5676	0.9002	0.6257	0.835	1.2467	1.0284	0.5329	0.8395
1FE6	0.6233	0.7476	0.7446	0.566	0.9196	0.6346	0.844	1.2637	1.0538	0.5477	0.8448
1FPR	0.6191	0.7465	0.7087	0.5595	0.8881	0.6044	0.8346	1.2355	1.0237	0.4709	0.8738
1H6T	0.6352	0.7475	0.7165	0.584	0.904	0.612	0.8448	1.2511	1.0406	0.5094	0.8444
1I4S	0.6171	0.7473	0.7293	0.5743	0.891	0.6061	0.835	1.2378	1.0275	0.4618	0.8607
1IQQ	0.6241	0.7592	0.7364	0.5769	0.8941	0.618	0.8376	1.2446	1.0318	0.5025	0.8496
1JLI	0.6259	0.7552	0.713	0.5588	0.9061	0.6132	0.8549	1.2531	1.0398	0.4898	0.8402
1K40	0.6316	0.7721	0.7132	0.5644	0.9128	0.6187	0.8454	1.2557	1.0494	0.5151	0.8589
1KS9	0.6312	0.7516	0.7088	0.5714	0.8841	0.5963	0.8295	1.2313	1.0236	0.4777	0.853
1KTE	0.6263	0.7528	0.7191	0.5752	0.9105	0.613	0.8456	1.2499	1.0427	0.4679	0.8602
1KUU	0.6271	0.7518	0.7173	0.576	0.9049	0.6121	0.8414	1.2561	1.0439	0.506	0.8444
1KXA	0.6344	0.7697	0.743	0.5903	0.8916	0.618	0.8265	1.241	1.0278	0.5448	0.8523
1MIX	0.6244	0.7618	0.7363	0.5812	0.9006	0.6193	0.8388	1.2453	1.0348	0.5339	0.8414
1MJY	0.6288	0.7617	0.7225	0.5737	0.8922	0.6105	0.8485	1.249	1.0304	0.4976	0.8506
1N12	0.628	0.7447	0.7435	0.5784	0.8954	0.5945	0.8445	1.2455	1.034	0.469	0.8625
1OO9	0.6281	0.7527	0.7213	0.582	0.9034	0.6098	0.844	1.2532	1.0427	0.4686	0.8563
1OOI	0.6103	0.7479	0.7132	0.5726	0.8982	0.6134	0.8378	1.2446	1.0323	0.4659	0.8571
1PHN	0.6216	0.7552	0.7165	0.57	0.8937	0.6079	0.8454	1.246	1.0302	0.4763	0.845
1RAL	0.6266	0.7465	0.7314	0.573	0.8897	0.6021	0.8208	1.2269	1.0271	0.4594	0.8533
1SUR	0.6324	0.7421	0.7244	0.557	0.9161	0.611	0.8541	1.2614	1.0514	0.4575	0.8538
1WUZ	0.6291	0.7476	0.7324	0.5695	0.9021	0.6068	0.8328	1.2512	1.0398	0.5292	0.8428
1WWB	0.6452	0.7348	0.7316	0.5761	0.9035	0.6377	0.8154	1.2497	1.0325	0.554	0.8487
1X0M	0.6283	0.7571	0.7349	0.5751	0.8899	0.6056	0.8419	1.2421	1.0245	0.4962	0.8393
1XGO	0.6122	0.7619	0.7091	0.5617	0.8925	0.6005	0.8376	1.2335	1.0262	0.4738	0.8533

Table 3: The average  $h(2)$  and standard deviation for all 11 items of 29 selected proteins

	Average of $H$	standard deviation of $H$
bonded potential	0.6269	0.0075
angle potential	0.7525	0.0088
dihedral potential	0.7262	0.0139
improper potential	0.5728	0.0087
electrostatic potential	0.8997	0.0095
Van der Waals potential	0.6135	0.0121
kinetic energy	0.8388	0.0086
total energy	1.2471	0.0292
potential energy	1.0350	0.0100
pressure	0.4968	0.0406
volume	0.8508	0.0317

Table 4: Exponent  $\lambda$  of visibility graph of time series for 29 proteins

PDB ID	Bond-p	ang-p	dih-p	imp-p	ele-p	Vdw-p	Kin-e	Tot-e	Pot-e	pre	vol
1A3H	0.2282	0.2192	0.2323	0.2365	0.2166	0.2366	0.2189	0.1356	0.1869	0.2328	0.2102
1BFG	0.2305	0.2314	0.214	0.2288	0.2116	0.2366	0.2203	0.1281	0.1929	0.2373	0.2015
1BSN	0.2205	0.2297	0.2301	0.2312	0.2194	0.2366	0.2185	0.1237	0.1925	0.2485	0.2049
2DN8	0.2363	0.229	0.234	0.2197	0.2237	0.2379	0.2238	0.129	0.1952	0.2411	0.2123
2DO7	0.236	0.221	0.219	0.2353	0.2102	0.234	0.2129	0.1249	0.1949	0.2464	0.2089
1F39	0.2316	0.2188	0.2303	0.2452	0.2085	0.239	0.2197	0.1237	0.1885	0.2294	0.2082
1FE6	0.2301	0.2191	0.2202	0.2356	0.2155	0.241	0.2262	0.1278	0.1906	0.2408	0.2113
1FPR	0.2438	0.2235	0.2184	0.2338	0.2195	0.2313	0.2183	0.1356	0.1969	0.2383	0.2031
1H6T	0.2418	0.2269	0.2256	0.2333	0.2176	0.2393	0.2273	0.1327	0.1922	0.2317	0.2104
1I4S	0.2298	0.2186	0.229	0.2322	0.2149	0.2316	0.2208	0.1314	0.2026	0.2391	0.2234
1IQQ	0.2294	0.2293	0.2331	0.2386	0.2066	0.2245	0.2166	0.1226	0.1788	0.236	0.2039
1JLI	0.2356	0.2289	0.2258	0.2465	0.2144	0.2334	0.2327	0.1233	0.1936	0.2333	0.214
1K40	0.231	0.2128	0.226	0.2244	0.2113	0.2369	0.2115	0.1287	0.1982	0.2358	0.2034
1KS9	0.2291	0.2232	0.2381	0.2286	0.2166	0.2459	0.215	0.1335	0.1995	0.2398	0.2101
1KTE	0.2388	0.2267	0.2306	0.2362	0.2132	0.2364	0.2124	0.1274	0.1902	0.2369	0.2021
1KUU	0.2253	0.2353	0.216	0.2304	0.2151	0.2308	0.2185	0.1299	0.1904	0.237	0.2082
1KXA	0.2239	0.2308	0.2211	0.2375	0.2164	0.2268	0.2233	0.1335	0.1855	0.2474	0.2043
1MIX	0.2261	0.2277	0.2263	0.2343	0.2156	0.2386	0.213	0.1288	0.1932	0.2374	0.2062
1MJY	0.2336	0.2155	0.2263	0.229	0.2132	0.2446	0.2228	0.1366	0.1993	0.2434	0.2109
1N12	0.236	0.234	0.2309	0.2349	0.2185	0.2254	0.2137	0.1365	0.1838	0.2414	0.2005
1OO9	0.233	0.222	0.235	0.2315	0.2101	0.2294	0.2164	0.1296	0.1943	0.2342	0.2108
1OOI	0.2263	0.2327	0.2214	0.2301	0.215	0.2387	0.2151	0.119	0.1819	0.2284	0.2116
1PHN	0.2233	0.2245	0.2259	0.2363	0.2108	0.2287	0.2292	0.1295	0.1943	0.2416	0.2067
1RAL	0.2302	0.2256	0.2278	0.241	0.2105	0.2318	0.2234	0.1323	0.1939	0.2416	0.2055
1SUR	0.2326	0.2239	0.2299	0.2345	0.2175	0.2402	0.2147	0.1212	0.1835	0.2467	0.207
1WUZ	0.2297	0.2239	0.2297	0.2296	0.212	0.2306	0.2219	0.1345	0.1906	0.2374	0.2083
1WWB	0.2247	0.2217	0.214	0.2291	0.2158	0.2311	0.219	0.1325	0.1918	0.2282	0.2127
1X0M	0.2353	0.223	0.2277	0.2268	0.2168	0.2388	0.2203	0.1266	0.1905	0.2382	0.2076
1XGO	0.2318	0.2154	0.2339	0.2301	0.2069	0.2296	0.2233	0.1263	0.1956	0.2354	0.2078

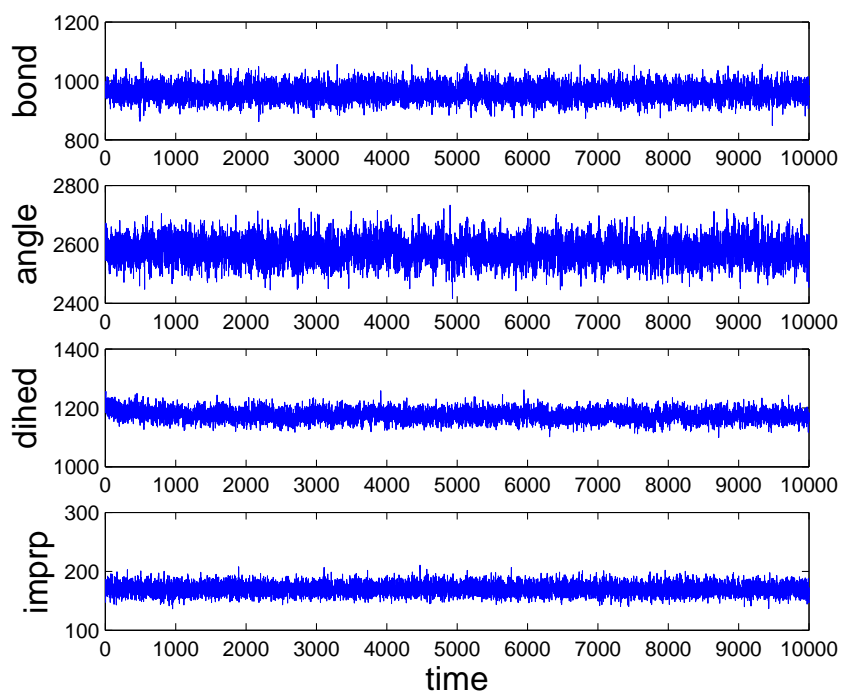


Figure 1: Bonded potential, angle potential, dihedral potential and improper potential time series for protein 1A3H.

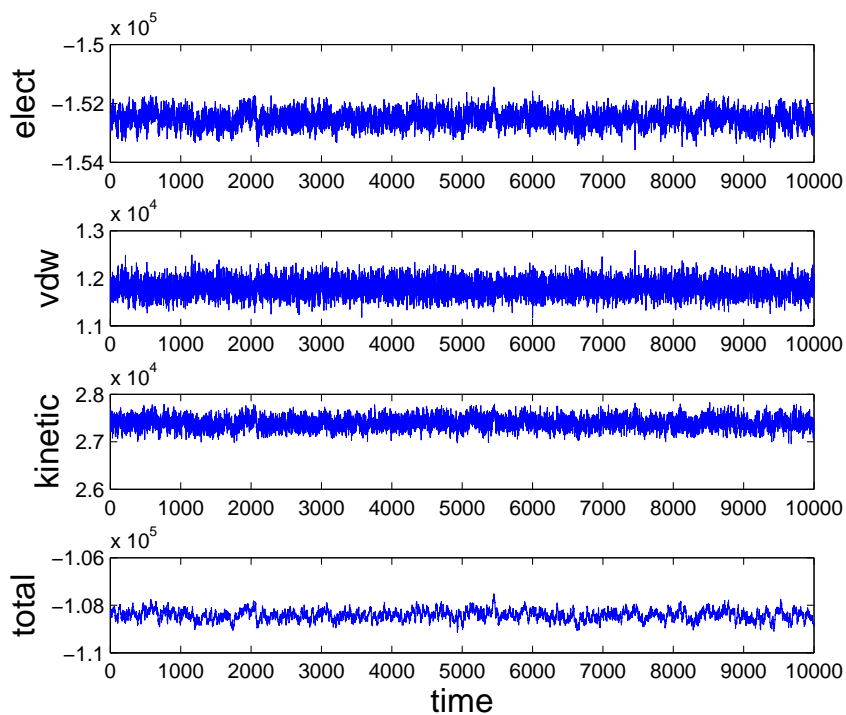


Figure 2: Electrostatic potential, Van der Waals potential, kinetic energy and total energy time series for protein 1A3H.

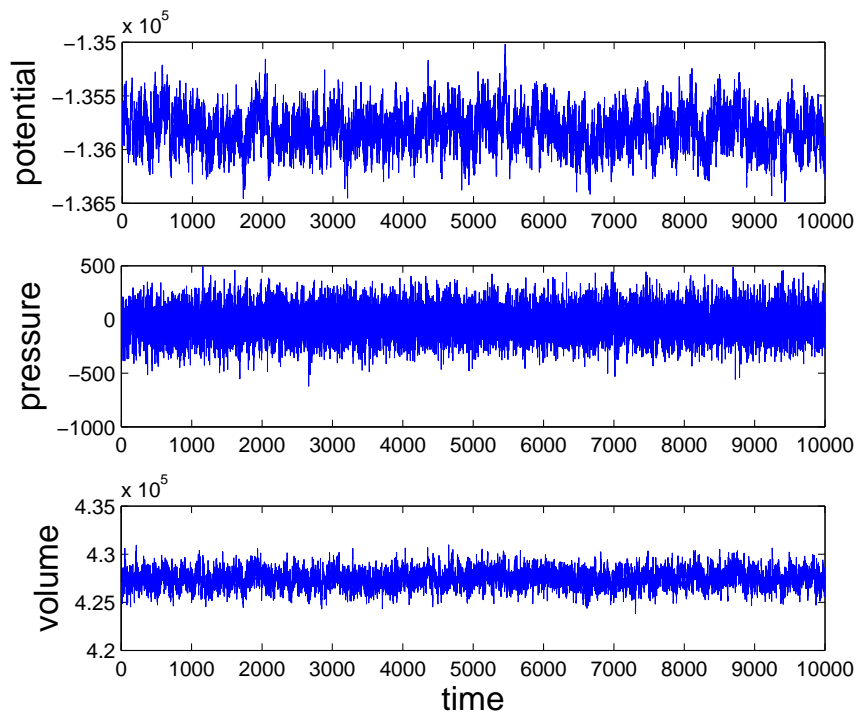


Figure 3: Potential energy, pressure, and volume time series for protein 1A3H.

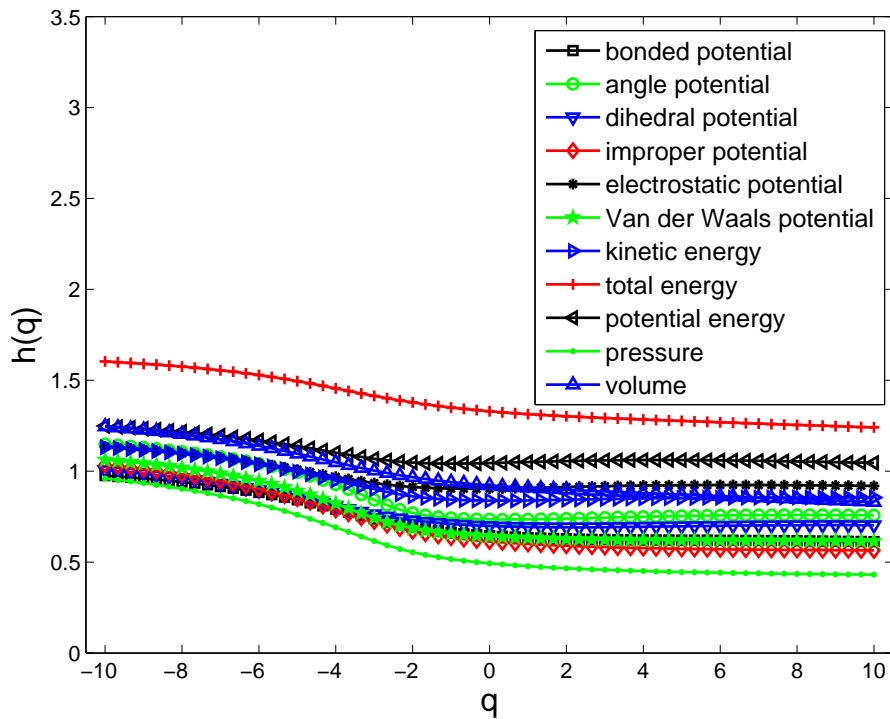


Figure 4: Multifractal  $h(q)$  curves of 11 time series for protein 1A3H.



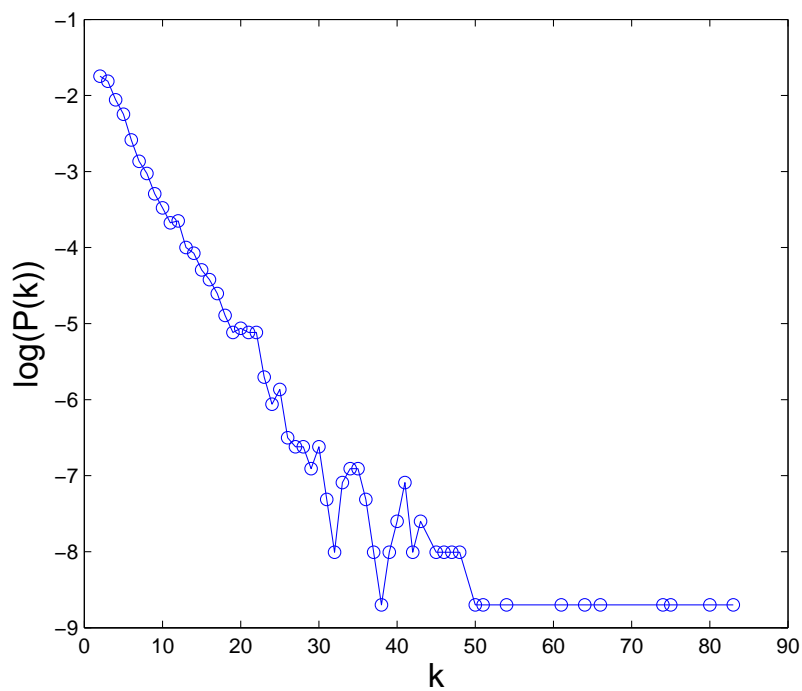


Figure 5: The degree distributions  $P(k)$  of visibility graph for potential energy time series of protein 1A3H.

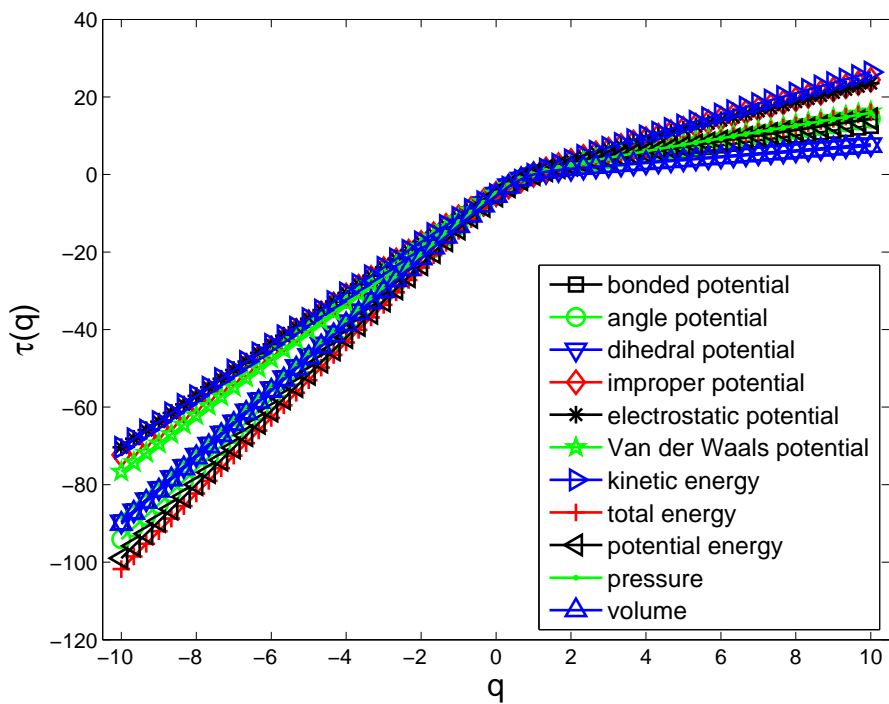


Figure 6: The  $\tau(q)$  curves of visibility graphs for energy, pressure and volume time series of protein 1A3H.

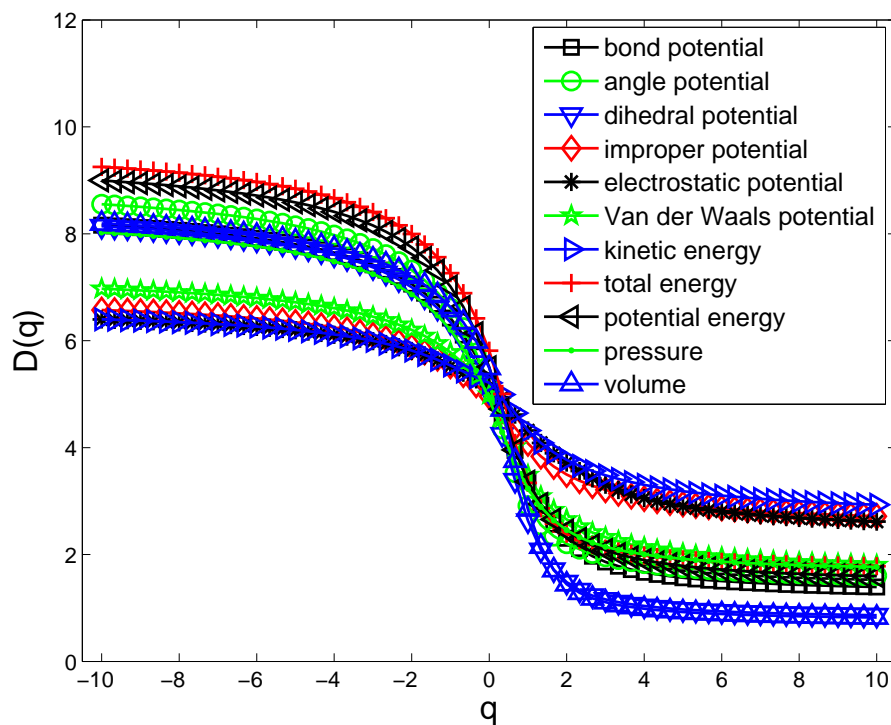


Figure 7: The  $D(q)$  curves of visibility graphs for energy, pressure and volume time series of protein 1A3H.

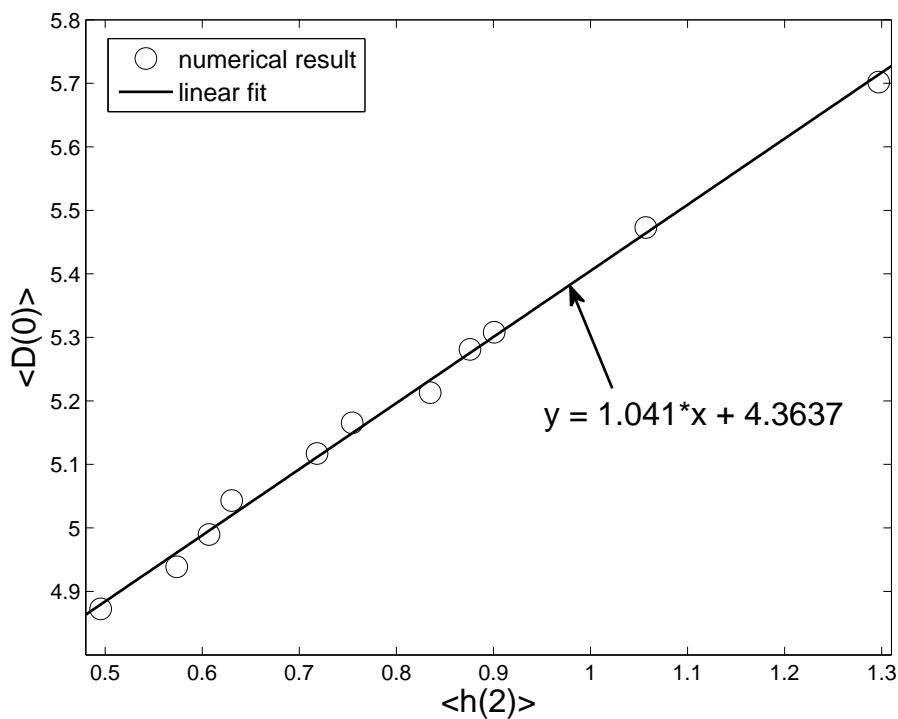


Figure 8: The relationship between  $\langle h(2) \rangle$  (from MF-DFA on time series) and  $\langle D(0) \rangle$  of the constructed visibility graphs for different energy, pressure and volume. The average is taken over 29 proteins.